King Saud University

**Arabian Journal of Chemistry**

www.ksu.edu.sa
www.sciencedirect.com

# ORIGINAL ARTICLE

# Synthesis, structure and anticancer studies of Cu (II), Ni (II) and Co (II) complexes based on 2,3-dihydroxybenzaldehyde-2-(2-aminophenyl) benzimidazole Schiff base

## Min Hou, Hou Cong Li, Ning An, Wen Ge Li *, Jing Tong *

*School of Basic Courses, Bengbu Medical College, Bengbu, China*
*Anhui Province Key Laboratory of Translational Cancer Research, Bengbu Medical College, Bengbu, China*

**Abstract** Three metal complexes [Cu(HL)Cl]($C_2H_5OH$)$_2$] (complex 1), [Ni$_4$L$_2$(CH$_3$COO)$_4$(C$_2$H$_5$-OH)$_4$] (complex 2) and [CoHL$_2$] (complex 3) based on 2,3-dihydroxybenzaldehyde-2-(2-aminophenyl)benzimidazole Schiff base (H$_2$L) were synthesized by solvothermal reaction. The three complexes were characterized by FT-IR spectrometer, elemental analysis, thermogravimetric analysis, and X-ray single-crystal diffraction. X-ray single-crystal diffraction analysis confirmed that complex 1 belongs to monoclinic crystal system with $P2_1/c$ space group, and complex 3 crystallizes in trigonal crystal system with R-3 space group. However, complex 2 crystallized in triclinic crystal system with P-1 space group and exhibits centrosymmetric tetranuclear crystallographic structure. Besides, MTT assay was studied antitumor activities against different tumor cells. The results show that the three complexes all have fine anticancer activities. Among them, complex 2 has significantly better anticancer properties against CNE-2Z cells than that of cisplatin. Finally, apoptosis and cell migration were studied to prove that complex 2 could inhibit tumor cells from proliferating in the manner of apoptosis and migration.

* Corresponding authors at: School of Basic Courses, Anhui Province Key Laboratory of Translational Cancer Research, Bengbu Medical College, Bengbu 233030, China.
E-mail addresses: 1686170071@qq.com (M. Hou), 540252947@qq.com (H.C. Li), 1299348081@qq.com (N. An), lwg1010@163.com (W. G. Li), 0200017@bbmc.edu.cn (J. Tong).

Production and hosting by Elsevier

## 1. Introduction

Currently, cancer is the major cause of human mortality, and a variety of treatments are used to fight the battle against cancer, in which chemotherapy is the most effective treatment to destroy cancer cells (Bray et al., 2018; Torre et al., 2016). Cisplatin is one of the earliest and most effective anticancer drugs. However, its drug resistance and nonspecific toxicity restrict its clinical application (Ghosh et al., 2019; Sun et al., 2019;

Köberle et al., 2010). Consequently, many non-platinum metal complexes were designed to develop anticancer drugs with high efficiency and few side effects. So far, the benzimidazole moiety is a key pharmacophore in medicinal industry due to its biological activities, such as anticancer, antibacterial, anti-inflammatory and analgesic effects (Yadav et al., 2015; Ates-Alagoz et al., 2016; Keri et al., 2015; Keri et al., 2016; Akhtar et al., 2017; Sirim et al., 2020). For instance, Hranjec M et al synthesized a series of novel benzimidazole Schiff bases. In vitro anticancer results showed that some of compounds exerted excellent inhibitory effect on HeLa and MCF-7 cell lines (Hranjec et al., 2011).

Schiff bases are a class of organic compounds formed by the condensation of amines with carbonyl groups. Owing to Schiff bases' lively imine groups, they are easily coordinated with metal ions to form various complexes. (Reshma et al., 2022; Kostova and Saso, 2013; Khan et al., 2022; Xu et al., 2020; Fontana et al., 2022). In addition, structural modifications of ligands are key aspects to the relations of their biological activities. Thus, a variety of benzimidazole Schiff base metal complexes are designed to improve their diverse biological activities as potential anticancer drugs (Casanova et al., 2018; Skrodzki et al., 2021; Magd-El-Din et al., 2018; Galal et al., 2009). Anup Paul et al prepared three benzimidazole-based Schiff base copper(II) complexes. Anticancer results showed one of Cu (II) complexes exhibits significant cytotoxic effect on A549 cancer cells. (Paul et al., 2015). Lotfi M et al synthesized benzimidazole schiff base ligand and its Cr (III), Mn (II) and Zn (II) metal complexes. The cytotoxicity results showed that Mn (II) complexes had good inhibitory effects on HCT 116 cells, HepG$_2$ cells and MCF-7 cell (Aroua et al., 2023).

Meanwhile, the current studies show that most of the benzimidazole Schiff base complexes do not have precise molecular structure and their anticancer activities need to be improved (Kumaravel et al., 2018; Tahlan et al., 2019; Aragón-Muriel et al., 2021). Non-platinum metal elements, such as copper, nickel, and cobalt are essential nutrients in the human body. In this paper, three new 2,3-dihydroxybenzaldehyde-2-(2-aminophenyl)benzimidazole Schiff base metal complexes [Cu(HL)Cl](C$_2$H$_5$OH)$_2$, [Ni$_4$L$_2$(CH$_3$COO)$_4$(C$_2$H$_5$OH)$_4$] and [Co(HL)$_2$] were synthesized by the solvothermal method. Their crystal structures were resolved by X-ray single crystal diffraction and their anticancer activities were also studied.

## 2. Experimental part

### 2.1. Materials and instruments

Chemical reagents and solvents were provided by Shanghai Aladdin Biochemical Technology Co. MTT reagents (Shanghai, China) were provided by BTS Biotech. Apoptosis assay kit (Nanjing, China) was provided by KeyGEN Biotech.

IR spectra were measured by Nicolet Model Nexus 470 FT-IR spectrometer, using KBr pellets. Elemental analyses for C, H, and N were carried out with Elementar Vario EL cube analyzer. X-ray crystallographic data were obtained from Bruker Apex APEX II X-ray single crystal diffractometer. Powder X-ray diffraction (PXRD) patterns were obtained on the

Bruker D8 diffractometer. TG was performed with STA 449-F3 instrument.

### 2.2. Synthesis of the Schiff base ligand

2-(2-aminophenyl)benzimidazole (2.0 g, 9.56 mmol) was added to 80 mL ethanol, then slowly dripped 2,3-dihydroxybenzaldehyde (1.32 g, 9.56 mmol) (Fig. 1). The mixture was refluxed for 4–5 h at 60 ℃ and obtained white precipitate. The white precipitate was filtered and then washed with cold ethanol. (Yield: 74.78%). $^1$H NMR: δ 9.69 (s, 1H), 9.16 (s, 1H), 7.97 (d, J = 7.6 Hz, 1H), 7.65 (d, J = 7.96 Hz 1H), 7.28—7.06 (m, 6H), 6.88 (d, J = 8.1 Hz, 1H), 6.80 (t, J = 7.48 Hz, 1H), 6.74 (d, J = 7.8 Hz, 1H), 6.45 (t, J = 7.9 Hz, 1H), 6.19 (t, J = 7.8 Hz, 1H) (Fig. S1). $^{13}$C NMR: δ 147.7, 145.9, 144.3, 144.0, 143.0, 133.4, 132.0, 127.5, 125.1, 122.6, 122.4, 119.7, 119.0, 118.3, 116.8, 116.0, 115.0, 112.0, 110.7, 63.2 (Fig. S2).

### 2.3. Synthesis of the Cu (II) complex

CuCl$_2$·2H$_2$O (0.005 g, 0.032 mmol), H$_2$L (0.02 g, 0.061 mmol), 0.01 mL triethylamine and 8 mL ethanol were mixed (Fig. 1). The reactants were transformed into a 20 mL teflon-sealed autoclave and subsequently heated to 75 ℃ for 3 d. Cooling down to room temperature, the dark green crystals were got. (Yield: 53.65%). C$_{24}$H$_{26}$ClCuN$_3$O$_4$(%): C: 55.49, H: 5.04, N: 8.09, Found: C: 55.57, H: 4.92, N:8.17. FT-IR (KBr, cm$^{-1}$): ν (O–H) 3615, ν (C = N) 1652, ν (C-O) 1176, ν (Cu–O) 517 (Fig. S3).

### 2.4. Synthesis of the Ni (II) complex

Ni(CH$_3$COO)$_2$·4H$_2$O (0.02 g, 0.080 mmol), H$_2$L (0.01 g, 0.030 mmol) and 0.03 mL triethylamine were added to 8 mL ethanol and heated at 70 ℃ for 4 d (Fig. 1). The yellow-green crystals were obtained by similar method to that of Cu (II) complex (Yield: 55.32%). C$_{56}$H$_{62}$N$_6$Ni$_4$O$_{16}$: C: 51.35, H: 4.77, N: 6.42, Found: C: 51.42, H: 4.70, N: 6.51. FT-IR (KBr, cm$^{-1}$): ν (O–H)3748, ν (C = N) 1634, ν (C-O)1079, ν (Ni-O) 504 (Fig. S4).

### 2.5. Synthesis of the Co (II) complex

CoCl$_2$·6H$_2$O (0.004 g, 0.017 mmol), H$_2$L (0.015 g, 0.046 mmol), 0.04 mL triethylamine, 5 mL ethanol, and 3 mL ethyl acetate were mixed fully, heated at 65 ℃ for 3 d (Fig. 1). Afterwards, the dark purple crystals were obtained by the same method as Cu (II) complex (Yield: 62.43%). C$_{40}$H$_{27}$CoN$_6$O$_4$: C: 67.23, H: 3.81, N: 11.76. Found: C: 67.16, H: 3.73, N: 11.89. FT-IR (KBr, cm$^{-1}$): ν (O–H) 3626, ν (C = N) 1617, ν (C-O) 1076, ν (Co-O) 502 (Fig. S5).

### 2.6. Structure determination

The single crystals were examined with a Bruker APEX II diffractometer. Software SAINT and SADABS were used to calibrate the data (BrukerSAINT, 2012). For the empirical adsorption correction, SADAB was employed. SHELX was
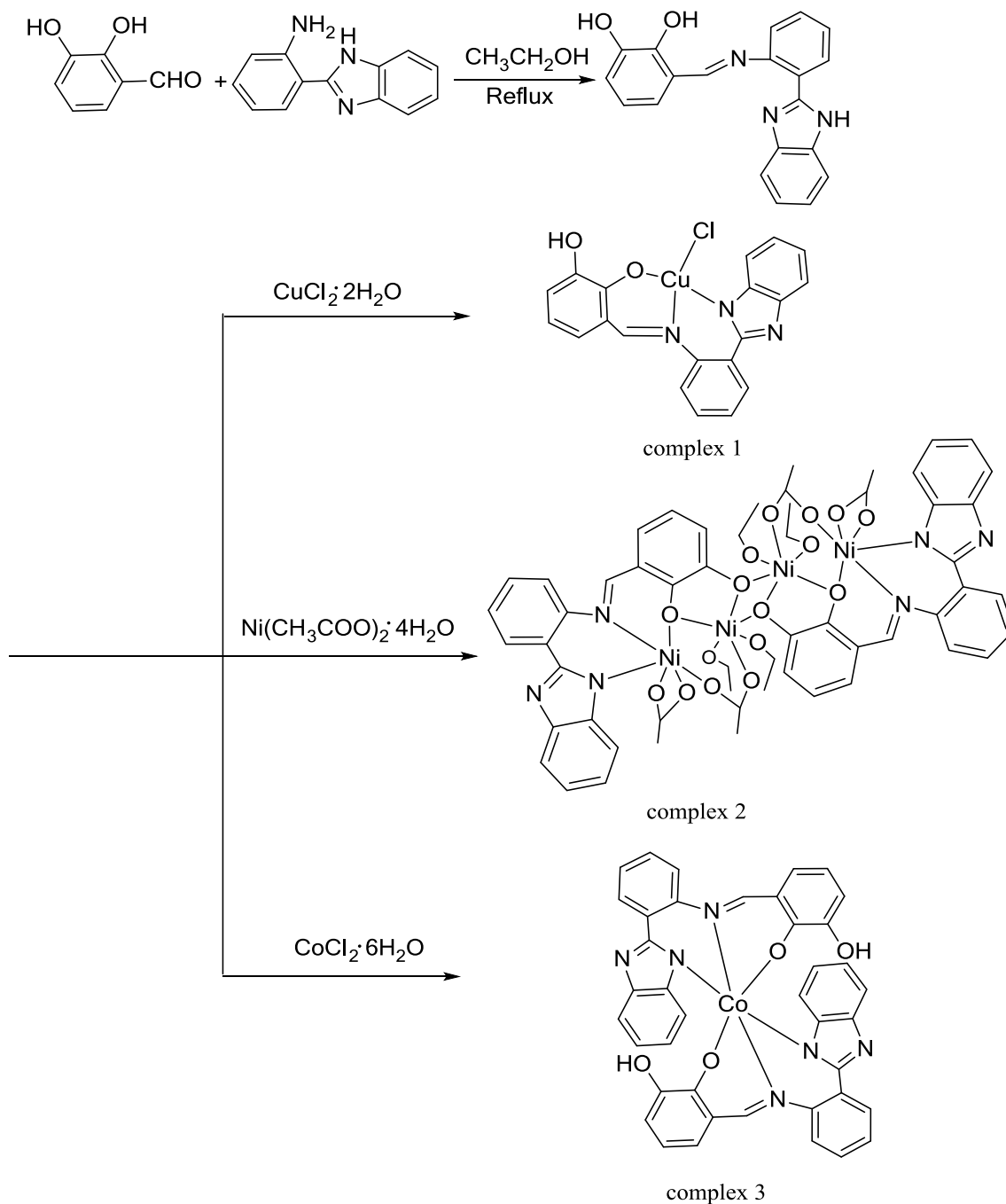
**Fig. 1** Synthetic pathway of ligand and complexes 1, 2 and 3.

employed to solve the structures (Krause. et al., 2015; Hübschle et al., 2011). Anisotropic displacement parameters were utilized to refine all atoms with the exception of H. Crystallographic data are shown in Table 1. The selected bond lengths and angles are shown in Table 2.

*2.7. Cytotoxicity assay (MTT)*

The antitumor activity of the three complexes on human MAD-MB-231, A549, CNE-2Z, and SMMC-7721 cells was determined by the MTT method. The cells were inoculated when the cell density reached 80% in every well. Then the compounds were diluted to different concentrations in the medium and added to 96-well plates. Meanwhile, cisplatin and DMSO were used as positive and negative controls, respectively. Cultivated (37 °C, 5% $CO_2$) for 72 h, 10 mL of MTT was added and incubated in a cell incubator for 4 h. After removing the culture medium, the formazan crystals were dissolved with 150 uL DMSO. The absorbance value at 490 nm was measured with a microplate reader, and then the $IC_{50}$ was calculated (Kumar et al., 2018).

**Table 1** Crystal parameters of complexes 1, 2 and 3.

| Complex | complex 1 | complex 2 | complex 3 |
|---|---|---|---|
| Empirical formula | $C_{24}H_{26}ClCuN_3O_4$ | $C_{56}H_{62}N_6Ni_4O_{16}$ | $C_{40}H_{27}CoN_6O_4$ |
| Molecular weight | 519.47 | 1309.88 | 714.60 |
| Crystal system | monoclinic | triclinic | trigonal |
| Crystal size($mm^3$) | $0.37 \times 0.23 \times 0.14$ | $0.07 \times 0.04 \times 0.03$ | $0.25 \times 0.23 \times 0.18$ |
| Space group | $P2_1/c$ | $P$-1 | $R$-3 |
| $\lambda/\text{Å}$ | 0.71073 | 0.71073 | 0.71073 |
| a (Å) | 12.7552(5) | 10.974(14) | 33.6912(8) |
| b (Å) | 13.5677(5) | 12.6947(13) | 33.6912(8) |
| c/(Å) | 14.3188(4) | 12.7848(19) | 17.9473(9) |
| $\alpha$(°) | 90 | 119.453(3) | 90 |
| $\beta$(°) | 112.033(2) | 99.642(5) | 90 |
| $\gamma$(°) | 90 | 101.753(4) | 120 |
| V ($\text{Å}^3$) | 2297.02(14) | 1441.6(3) | 17642.6(12) |
| Z | 4 | 1 | 18 |
| $\rho$calc.($g \cdot m^{-3}$) | 1.502 | 1.509 | 1.211 |
| angles of data collected | 0.65–0.75 | 0.60–0.75 | 0.66 – 0.75 |
| $\mu$($mm^{-1}$) | 1.104 | 1.360 | 0.483 |
| F(000) | 1076 | 680 | 6624 |
| Data/restraint/parameters | 4156/ 75/ 344 | 4929/ 3/ 383 | 7106 / 0 / 460 |
| Goodness − of − fit on $F^2$ | 1.053 | 1.033 | 1.050 |
| R indexes [all data] | $R_1 = 0.0417$ $wR_2 = 0.0804$ | $R_1 = 0.1427$ $wR_2 = 0.0924$ | $R_1 = 0.1090,$ $wR_2 = 0.1597$ |
| Final R1, wR2[I > =2σ (I)] | 0.0307, 0.0732 | 0.0658, 0.0792 | 0.0510, 0.1263 |
| Largest diff. peak/hole / $e\text{Å}^{-3}$ | 0.749 and −0.306 | 0.632 and −0.625 | 0.460 and −0.440 |
| CCDC No | 2,244,067 | 2,244,085 | 2,244,086 |

**Table 2** Complexes 1,2and 3 selected bond lengths (Å) and angles (°).

complex 1

| | | | | | |
|---|---|---|---|---|---|
| Cu1 − Cl1 | 2.297(6) | O2 − Cu1 − Cl1 | 157.8(8) | N1 − Cu1 − Cl1 | 93.8(6) |
| Cu1 − O2 | 1.889(1) | O2 − Cu1 − N3 | 94.5(7) | N3 − Cu1 − Cl1 | 155.2(6) |
| Cu1 − N1 | 1.947(1) | N1 − Cu1 − N3 | 91.0(8) | | |
| Cu1 − N3 | 1.985(1) | O2 − Cu1 − Cl1 | 90.1(5) | | |

complex 2

| | | | | | |
|---|---|---|---|---|---|
| Ni1 − O2 | 1.997(4) | O2 − Ni1 − O3 | 98.4(1) | O1 − Ni2 − O1 | 84.4(1) |
| Ni1 − O3 | 2.026(4) | O2 − Ni1 − O5 | 94.0(1) | O2 − Ni2 − O4 | 104.8(1) |
| Ni1 − O5 | 2.139(5) | O2 − Ni1 − O6 | 154.6(1) | O2 − Ni2 − O7 | 160.4(1) |
| Ni1 − O6 | 2.241(5) | O2 − Ni1 − N1 | 90.9(1) | O2 − Ni2 − O8 | 87.7(1) |
| Ni1 − N1 | 1.997(6) | O2 − Ni1 − N2 | 103.5(1) | O1 − Ni2 − O2 | 79.8(1) |
| Ni1 − N2 | 2.015(5) | O3 − Ni1 − O5 | 91.2(1) | O4 − Ni2 − O7 | 93.3(1) |
| Ni2 − O1 | 2.009(4) | O3 − Ni1 − O6 | 84.1(2) | O4 − Ni2 − O8 | 87.8(1) |
| Ni2 − O2 | 2.134(5) | O3 − Ni1-N1 | 169.4(1) | O4 − Ni2 − O1 | 90.5(1) |
| Ni2 − O4 | 2.026(4) | O3 − Ni1 − N2 | 89.9(2) | O7 − Ni2 − O8 | 85.6(1) |
| | | O5 − Ni1 − O6 | 60.5(1) | O7 − Ni2 − O1 | 94.0(1) |
| | | O5 − Ni1 − N1 | 93.2(1) | O8 − Ni2 − O1 | 178.4(1) |
| | | O5 − Ni1 − N2 | 162.0(1) | O1-Ni2-O4 | 173.3(1) |
| | | O6 − Ni1 − N1 | 89.6(1) | O1 − Ni2 − O7 | 82.7(1) |
| | | O6 − Ni1 − N2 | 101.7(1) | O1 − Ni2 − O8 | 97.0(1) |
| | | N1 − Ni1 − N2 | 83.0(1) | O1 − Ni2 − O2 | 79.8(1) |

complex 3

| | | | | | |
|---|---|---|---|---|---|
| Co1 − O4 | 1.893(2) | O4 − Co1 − O2 | 87.5(1) | O2 − Co1 − N1 | 90.0(1) |
| Co1 − O2 | 1.903(3) | O4 − Co1 − N6 | 92.1(1) | N6 − Co1 − N1 | 90.7(1) |
| Co1 − N6 | 1.921(3) | O2 − Co1 − N6 | 174.9(1) | N4 − Co1 − N1 | 93.9(1) |
| Co1 − N4 | 1.921(3) | O4 − Co1 − N4 | 90.9(1) | N3 − Co1 − N1 | 85.8(1) |
| Co1 − N3 | 1.931(3) | O2 − Co1 − N4 | 90.3(1) | N6 − Co1 − N3 | 94.5(1) |
| Co1 − N1 | 1.944(3) | N6 − Co1 − N4 | 84.6(1) | N4 − Co1 − N3 | 179.2(1) |
| | | O4 − Co1 − N3 | 89.2(1) | O4 − Co1 − N1 | 174.5(1) |
| | | O2 − Co1 − N3 | 90.4(1) | | |

## 2.8. Cell migration

The migratory ability of the complexes was studied against CNE-2Z cells. Cells in the logarithmic growth phase were collected, centrifuged, and resuspended in medium containing 10% serum. Subsequently, cells were seeded in 6-well plates and incubated at 37 ℃, 5% $CO_2$. When the cells density grew to 90%, a straight line was drawn in the central area, and the suspended cells were gently washed away twice with PBS. Different concentrations of the complexes were prepared with 4% serum in the medium and then added to a 6-well plates. Pictures of the migration were taken at 0, 12, and 48 h with an inverted microscope (Peng et al., 2022).

## 2.9. Exploration of apoptosis

Cell apoptosis of CNE-2Z cells was tested by Annexin-VFITC/ PI method. The labeled Annexin V can be used as a probe to detect the changes of cell membrane caused by apoptosis, which can be used for examining apoptotic cells. Cells were seeded at a density of $1 \times 10^6$ cells/well in a 6-well plate and cultured (37 ℃, 5% $CO_2$) for 24 h. CNE-2Z cells were treated with different concentrations of Ni (II) complexes for 24 h.

After trypsinization without EDTA, the cells were colllected by centrifugation. Then washed twice with cold PBS and centrifuged for 5 min at 2000 r. 400 uL of Binding Buffer solution was added to resuspend cells, and then 5 uL of FITC and 10 uL of PI were added to the cell suspension in turn, mixing them gently. Next, cells were incubated for 5–10 min at room temperature in a dark environment. The cells were detected by flow cytometry (FACS) within 1 h (Wang et al., 2022).

## 2.10. Statistical analysis

The experimental data were analyzed and processed using SPSS 19.0 statistical software and expressed as mean ± SD. The differences between groups were compared by one-way ANOVA (One-way ANOVA) and $t$-test, and $P < 0.05$ was considered statistically significant between the two groups.

## 3. Results and discussion

### 3.1. Crystal structure analysis

Complex 1 crystallizes in tetragonal structure with space group $P2_1/c$ (Table 1). As shown in Fig. 2a, the tetra-coordinate cen-
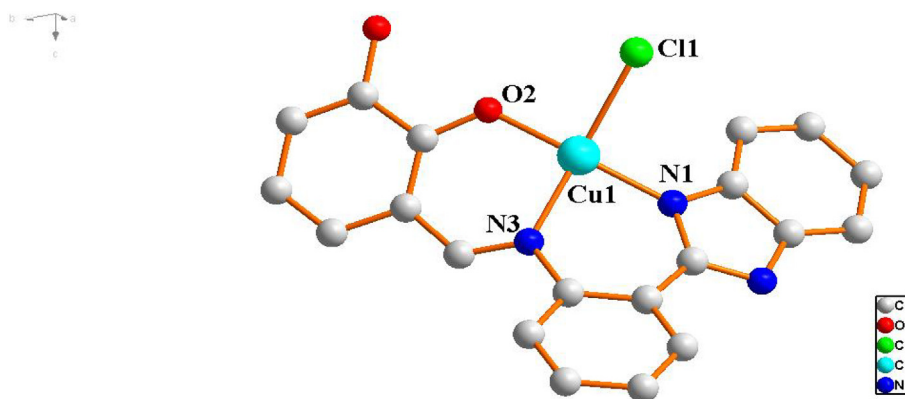


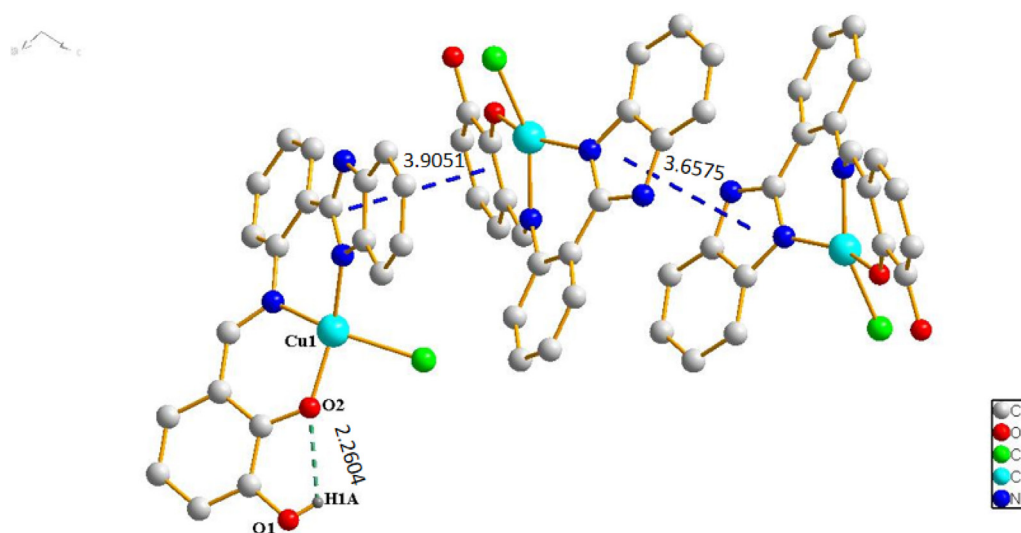**Fig. 2a**   The molecular structure of the Cu (II) complex 1.



**Fig. 2b**   Hydrogen bonds (green dashed lines) and πṡṡṡπ interactions (blue dashed lines) in Cu (II) complex 1.
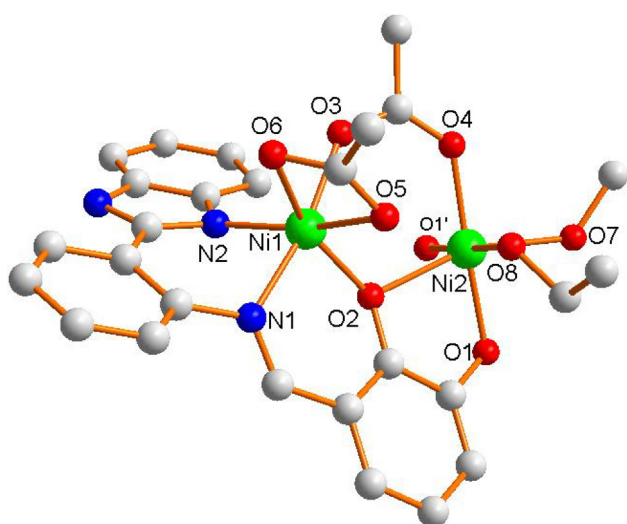
**Fig. 3a**  The asymmetric unit of the Ni (II) complex 1.

ter Cu (II) ion is coordinated to N1, N3 O2 and Cl1 forming planar quadrilateral structure. Among which N1 and N3 atoms are from the C = N bond and imidazole of one 2,3-dihy droxybenzaldehyde-2-(2-aminophenyl)benzimidazole Schiff base ligand, O2 is from the hydroxyl group of the same Schiff base ligand and Cl1 is from copper chloride. As a result of the bond angles of tetra-coordinate center Cu (II) ion are ∠N1 − Cu1 − Cl1 = 93.8(2)°, ∠N3 − Cu1 − O2 = 94.5(7 )°, ∠N3 − Cu1 − N1 = 91.0(8)° and ∠O2 − Cu1 − Cl1 = 90.1(5)° respectively, constructing a slightly distorted planar square geometry. The stacking diagram of complex 1 reveals that imidazole (benzene) rings of Schiff base ligands are parallel to the other adjacent imidazole (benzene) rings of Schiff base ligands, forming face-to-face (3.6575 Å, 3.9051 Å) intermolecular stacking (Fig. 2b). There are intramolecular hydrogen bonds O—H⋯O (D H1A⋯O2 = 2.2604 Å) in complex 1. Finally, the complex 1 forms three-dimensional structure

through intermolecular π⋯π stacking interactions and hydrogen bonding.

Complex 2 belongs to trigonal system with *P*-1 space group (Table 1). Its independent molecular unit is made up of four Ni (II) ions, two Schiff base ligands ($L^{2-}$), four $CH_3COO^-$ ions, and four $C_2H_5OH$ molecules. As illustrated in Fig. 3a, its asymmetric unit contains two Ni (II) ions, one Schiff base ligand ($L^{2-}$), two $CH_3COO^-$ ions, and two $C_2H_5OH$ molecules. The two asymmetric units exhibit the same coordination structural environment. Ni1 ion is coordinated by O3, O5 and O6 (from the carboxyl groups of two different acetate ions), O2 (from one hydroxyl of Schiff base ligand), N1 (from C = N bond of Schiff base ligand) and N2 (from imidazole of Schiff base ligand) to form six-coordinated octahedral structure. The bond angles of central Ni1(II) ion are ∠N1-Ni1-O6 = 8 9.6(1)°, ∠O6-Ni1-O3 = 84.1(2)°, ∠O3-Ni1-O2 = 98.4(2)°, and ∠O2-Ni1-N1 = 90.9(1)° respectively, indicating N1, O2, O3, and O6 atoms are located in an approximate plane. Therefore, the six-coordinated [Ni1O4N2] moiety forms a distorted octahedron. In Fig. 3b, the Ni2 ion is coordinated by O1 and O2 (from two hydroxys of one Schiff base ligand), O4 (from carboxyl groups of the acetate ion), O7 and O8 (from two ethanol molecules) and O1′ (from one hydroxys of the other Schiff base ligand) to form the similar octahedral structure. Owing to the approximate plane, the [Ni2O6] moiety also forms a slightly distorted octahedron geometry. Ni1 and Ni2 atoms are bridged by O3, O4 (from one acetate ion) and O2 (from one hydroxy of Schiff base ligand) to form a distorted hexagon structure geometry. Finally, Ni2 and Ni2′ atoms are bridged by two O1 and O1′ atoms of hydroxy from two different Schiff base ligands to form centrosymmetric independent unit.

As depicted in Fig. 3c, the imidazole ring of the molecule is almost parallel to the benzene ring of the adjacent complex molecule, forming face-to-face (3.7905 Å) intermolecular stacking. There are intramolecular hydrogen bonds (O-H⋯O, D H7A⋯O2 = 2.2232 Å, DH8A⋯O5 = 1.8969 Å) and intermolecular hydrogen bonds (N-H⋯O, D H3A⋯O6 = 1.9546 Å) in complex 2. Ultimately, complex 2
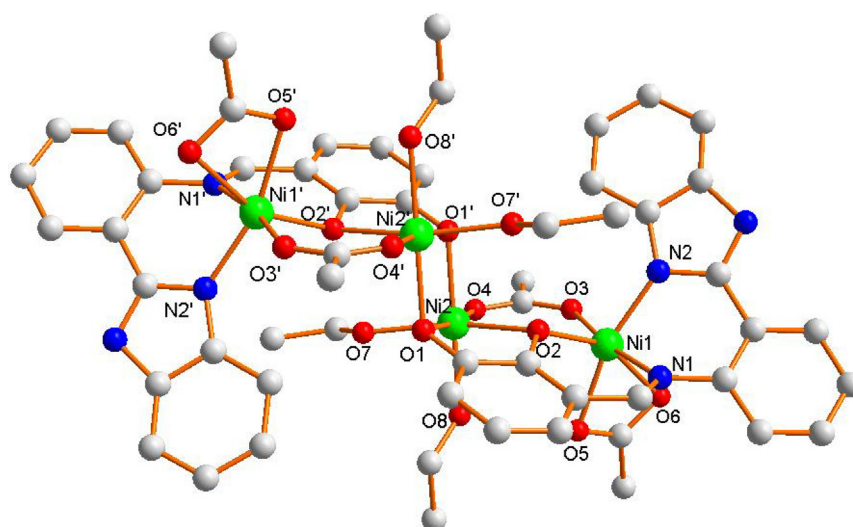


**Fig. 3b**  Molecular structure of ni (ii) complex 2.
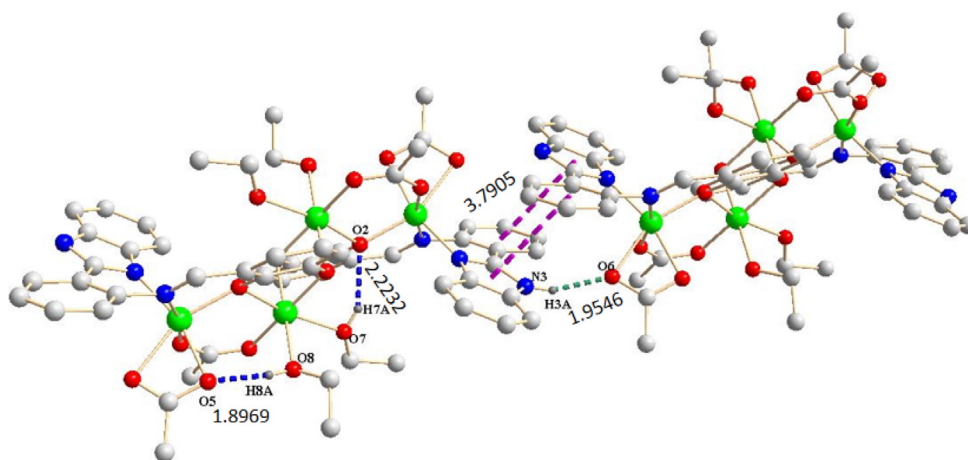
**Fig. 3c** Hydrogen bonds (blue,green dashed lines) and π⋯π interactions(purple dashed lines) in Ni(II) complex 2.
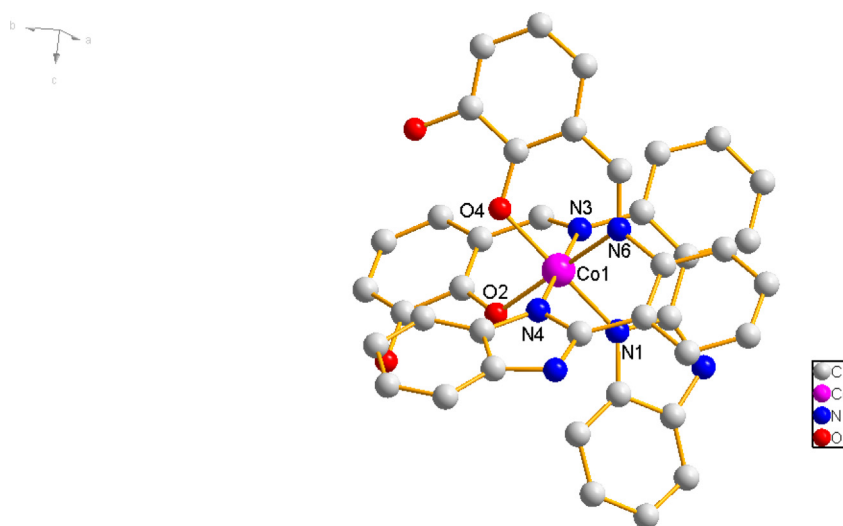


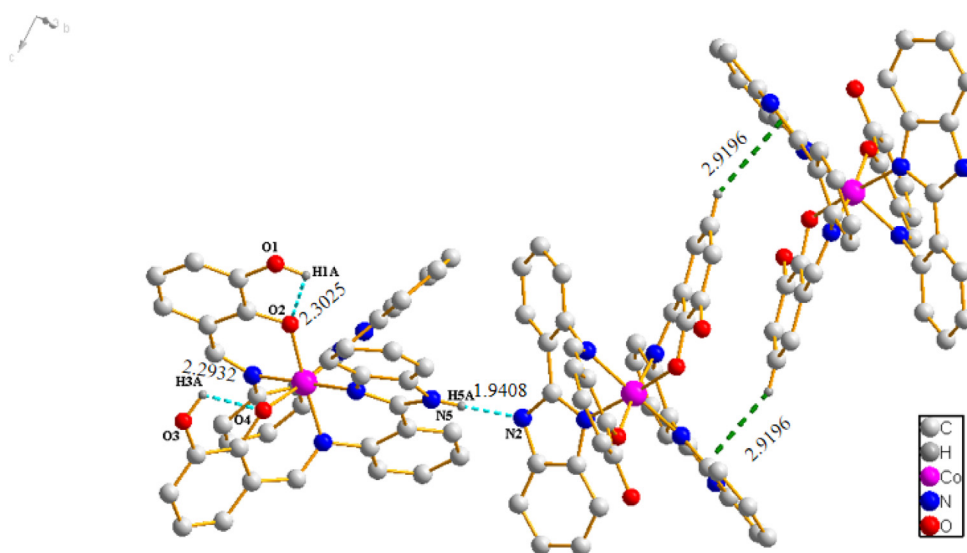**Fig. 4a** Molecular structure of co (ii) complex 3.



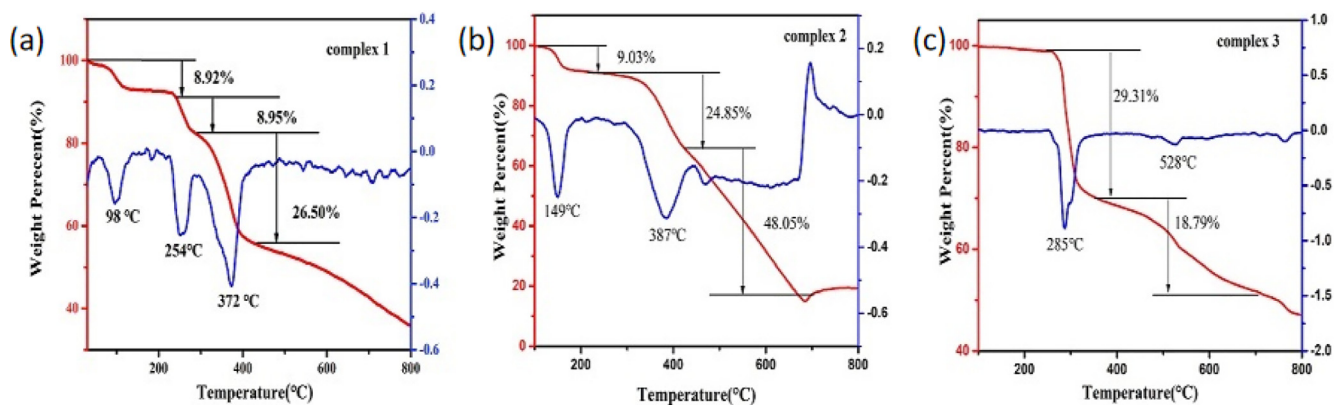**Fig. 4b** Hydrogen bonds (cyan dashed lines) and C-H⋯π interactions (green dashed lines) in Co (II) complex 3.

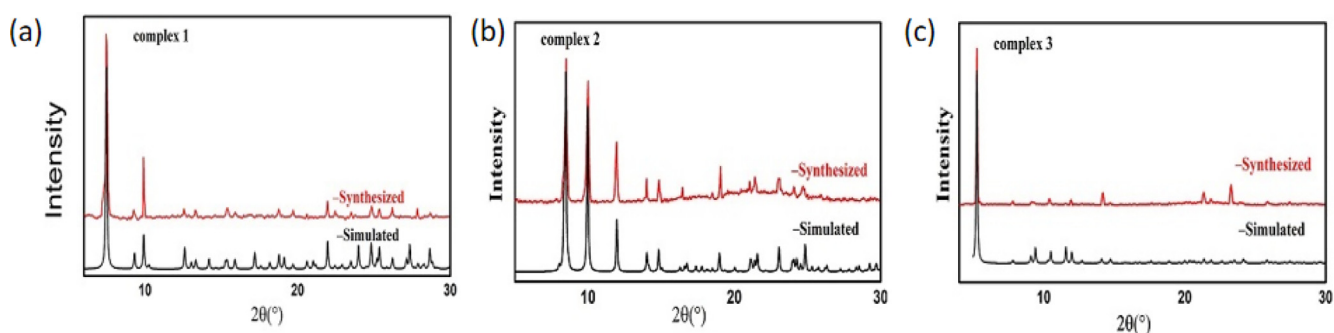**Fig. 5**    TG and DTG curves of complexes 1, 2 and 3.



**Fig. 6**    XRD patterns of complexes 1, 2 and 3 (Black- simulated from CIFs, Red-experimentally synthesized).

**Table 3**    IC$_{50}$ values of the ligand and complexes against four human tumor cells (A549, SMMC-7721, MDA-MB-231 and CNE-2Z cells.

| Compounds | IC$_{50}$ ($\mu$M $\pm$ SD) | | | |
|---|---|---|---|---|
| | CNE $-$ 2Z | MDA $-$ MB $-$ 231 | A549 | SMMC $-$ 7721 |
| complex 1 | 20.05 $\pm$ 0.72 | 15.43 $\pm$ 0.48 | 37.72 $\pm$ 0.65 | 54.79 $\pm$ 1.12 |
| complex 2 | 1.99 $\pm$ 1.60 | 8.84 $\pm$ 0.30 | 23.14 $\pm$ 2.73 | 21.50 $\pm$ 1.07 |
| complex 3 | 17.18 $\pm$ 0.14 | 15.98 $\pm$ 0.78 | 43.34 $\pm$ 0.60 | 73.10 $\pm$ 2.01 |
| H$_2$L | 24.36 $\pm$ 2.02 | 38.79 $\pm$ 0.79 | 100.69 $\pm$ 1.99 | 41.03 $\pm$ 1.50 |
| Cisplatin | 4.54 $\pm$ 0.04 | 4.02 $\pm$ 0.08 | 15.74 $\pm$ 0.54 | 4.42 $\pm$ 0.11 |

forms three-dimensional structure through $\pi\dot{s}\dot{s}\dot{s}\pi$ stacking and intramolecular hydrogen bonding interaction.

Complex 3 crystallizes in tripartite system with R-3 space group (Table 1). Complex 3 is six-coordinated octahedral configuration, in which central Co (II) ion is coordinated by N1, N4 from two benzimidazole ring of two Schiff base ligands, N3, N6 from two imine group of two Schiff base ligands and two O2, O4 from hydroxyl of two different Schiff base ligands, respectively (Fig. 4a). The bond angles of central Co (II) ion are $\angle$N6 $-$ Co1 $-$ N4 = 84.6(1)°, $\angle$N6 $-$ Co1 $-$ O4 = 92.1 (1)°, $\angle$N4 $-$ Co1 $-$ O2 = 90.3(1)°, and $\angle$O2 $-$ Co1 $-$ O4 = 87.5(1)° respectively. As a result, the [ Co N1 N6 O2 O4] moiety is located in an approximate plane geometry. Eventually, the Co (II) forms a slightly distorted

octahedral geometry. Their bond lengths Co1-N1 = 1.944(3) Å, and Co1-N6 = 1.921(3) Å, and Co1-O2 = 1.903(3) Å and Co1-O4 = 1.893(2) Å are in normal range.

As shown in Fig. 4b, there are intramolecular hydrogen bonds (O-H$\dot{s}\dot{s}\dot{s}$O, D H1A$\dot{s}\dot{s}\dot{s}$O2 = 2.3025 Å, D H3A$\dot{s}\dot{s}\dot{s}$O4 = 2.2932 Å) and intermolecular hydrogen bonds (N-H$\dot{s}\dot{s}\dot{s}$N, D H5A$\dot{s}\dot{s}\dot{s}$N2 = 1.9408 Å) within the complex 3. The complex 3 produce C-H$\dot{s}\dot{s}\dot{s}\pi$ stacking interactions, which the phenyl ring of 2,3-dihydroxysalicylaldehyde from one ligand is approximately perpendicular to the imidazole ring of 2-(2-aminophenyl)benzimidazole from the other, with an edge-to-face distance of 2.9196 Å. At last, the complex 3 monomer molecules are connected through C-H$\dot{s}\dot{s}\dot{s}\pi$ interactions and intermolecular hydrogen bonds.

## 3.2. Thermal stability of complexes 1, 2 and 3

As shown in Fig. 5a, the TG-DTG curves of the three complexes were studied. The weight loss process consists of four steps in complex 1. Firstly, the two weight losses are 8.92% and 8.95%, corresponding to loss of two coordinated ethanol molecules (98 ℃, 254 ℃), respectively. Secondly, the three weight loss is 26.5%, assigning to lose 2,3-dihydroxybenzaldehyde in 293 to 437 ℃ range. Finally, the skeleton of the complex 1 collapses and decomposes in 437 to 800 ℃ range. As shown in Fig. 5b, there are three weight loss steps in complex 2, in which weight losses are 9.03% (149 ℃), 24.84% (149 to 387 ℃) and 48.05% (387 to 685 ℃) respectively. The three weight losses correspond to the departure of two coordinated acetate ions, one 2,3-dihydroxybenzaldehyde-2-(2-aminophenyl)benzimidazole Schiff base ligand
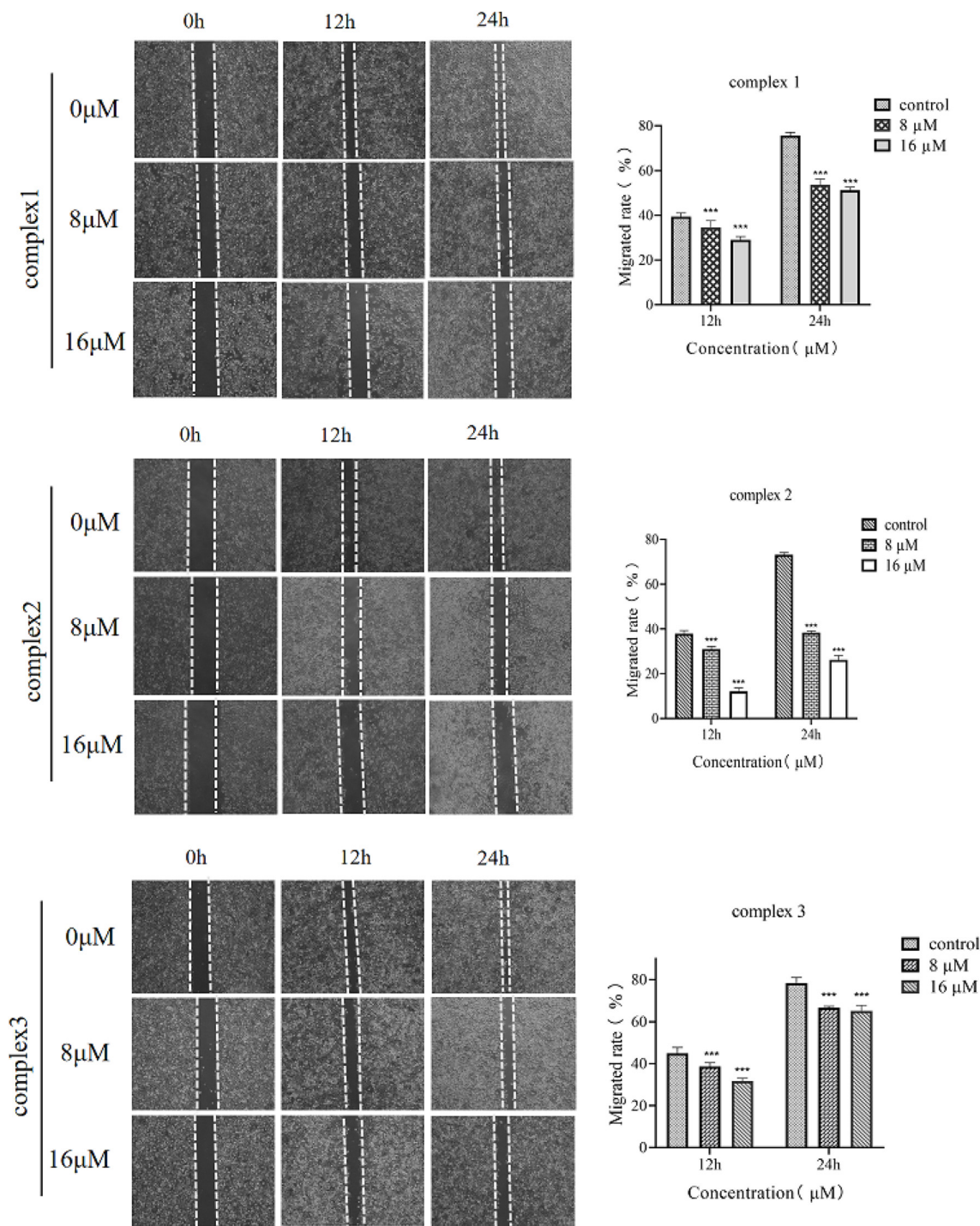


**Fig. 7** Effect of complex 1, complex 2 and complex 3 on the migration ability of CNE-2Z cells. Data represent mean ± SD (n = 3) and use one-way ANOVA with Tukey's multiple comparison test, ***$p < 0.005$ vs. Control.
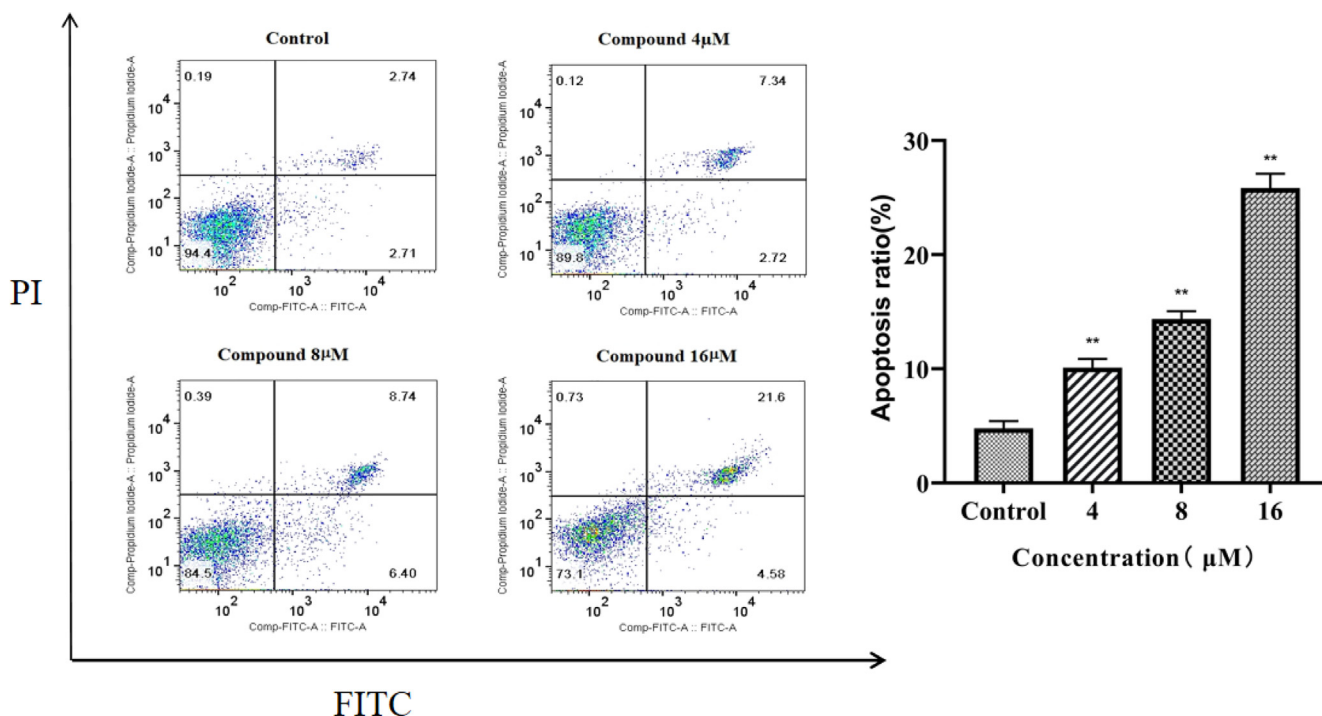
**Fig. 8** The effect of complex 2 on CNE − 2Z cell apoptosis rate: a Effect of different concentrations of complex 2 on apoptosis of CNE-2Z cells for 24 h. Apoptosis rate of complex 2 at 0 µM, 4 µM, 8 µM, and 16 µM (**P < 0.05).

molecule, and the other 2,3-dihydroxybenzaldehyde-2-(2-aminophenyl)benzimidazole Schiff base ligand molecule, two coordinated ethanol molecules, and four coordinated acetate ions, respectively. Complex 2 produces stable residues above 685°C. Complex 3 also takes place in three stages, corresponding to losses of mass of 29.31% (285 ℃) and 18.79% (356 to 528 ℃), respectively (Fig. 5c), attributed to eliminating 2,3-dihydroxybenzaldehyde-2-(2-aminophenyl)benzimidazole Schiff base ligand, and 2,3-dihydroxybenzaldehyde. Complex 3 is inconstant in the third stage above 528 ℃. According to TG-DTG curves of the three complexes, complex 3 has higher thermal stability than complex 1 and complex 2.

### 3.3. Powder XRD patterns of complexes 1,2 and 3

The powder XRD patterns of complex 1, 2 and 3 was further investigated by powder X-ray diffraction (PXRD) (Fig. 6). The intensities of diffraction peaks of complex 1, 2 and 3 are in accordance with their theoretical diffraction peaks generated from single crystal X-ray analysis. This indicates that the crystal samples of the three complexes conform to the crystal structures determined by single crystal analysis.

### 3.4. Cytotoxicity assay (MTT)

The anticancer effect of the compounds was evaluated against the human cancer cell lines and the IC$_{50}$ values are in Table 3. The results indicate that complex1-3 exhibit greater anticancer activity than ligand. Among them, complex 2 shows stronger anticancer activity than the other two complexes against four human cancer cell lines. Meanwhile, complex 2 exhibits lower

cytotoxicity than cisplatin on CNE-2Z cells. It may be related to the tetranuclear complex of complex 2.

### 3.5. CNE-2Z cell migration were inhibited by complexes

The effect of complexes 1, 2 and 3 against the migration of CNE-2Z cells was observed using a wound-healing assay. According to Fig. 7, complex 1 was applied to CNE-2Z cells at 0 µM, 8 µM and 16 µM. After 24 h, the cell migration rates were 75.64%, 53.68%, and 46.31%, respectively. Complex 2 was applied to CNE-2Z cells at concentrations of 8 µM and 16 µM. After 24 h, the cell migration rates were 37.90% and 26.30%, respectively. Similarly, for complex 3, at 0 µM, 8 µM and 16 µM, the cell migration rates were 44.88%, 38.63% and 31.64% respectively after 12 h. The cell migration rate was more than 65% at 24 h. According to the results of the study, complex 2 inhibits the lateral migration ability in a concentration-dependent manner, complex 1 can inhibit the migration of CNE-2Z cells at high concentrations, and complex 3 has little effect on the migration ability of CNE-2Z cells at low or high concentrations.

### 3.6. Cells apoptosis

To further investigate the inhibitory effect of complex 2 on CNE-2Z cells, the FITC-PI double staining method was used in this experiment to study. The effect of different concentrations of complex 2 on the apoptosis of CNE-2Z cells for 24 h (Fig. 8). Approximately 10.06%, 15.14% and 26.10% of apoptotic cells were observed when CNE-2Z cells were treated with 4 µM, 8 µM and 16 µM of complex 2, respectively.

This shows that complex 2 can significantly stimulate apoptosis of CNE-2Z cells with increasing concentration, and the effect is proportional to the concentration of the Ni (II) complex.

## 4. Conclusion

In our study, 2-(2-aminophenyl)benzimidazole and 2,3-dihydroxybenzaldehyde were used to synthesize schiff base ligand, and three metal complexes [Cu(HL)Cl](C$_2$H$_5$OH)$_2$, [Ni$_4$L$_2$(CH$_3$COO)$_4$(C$_2$H$_5$OH)$_4$] and [Co(HL)$_2$] were obtained by solvothermal method. X-ray single crystal diffraction analysis confirmed that Cu (II) complex is tetra-coordinated mononuclear, Ni (II) complex is six-coordinated tetranuclear molecule, and Co is tetra-coordinated mononuclear complex. MTT assay was studied for anticancer activities against different cancer cells. The anticancer activities of the three complexes are significantly better than that of the Schiff base ligand. It is worth mentioning that the anti-proliferative activity of complex 2 against CNE-2Z cells is better than that of cisplatin. Cell scratch assay shows that migration ability against CNE-2Z cells for complex 2 is high relative to increasing concentration. The results of apoptosis experiments also showed that complex 2 can significantly promote the apoptosis of CNE-2Z cells, and the apoptosis rate is proportional to the drug concentration.

## Declaration of Competing Interest

The authors declare that they have no known competing financial interests or personal relationships that could have appeared to influence the work reported in this paper.

## Acknowledgments

## Author contributions

**Min Hou:** Performed the research, wrote the paper and financial support. **Hou Cong Li:** Synthesized the complexes. **Ning An:** performed the PXRD and TGA tests.**Wen Ge Li\*:** Designed the research, performed the crystal structure study, wrote the paper and financial support. **Jing Tong\*:** Designed the research, performed the crystal structure study, wrote the paper and financial support.

## Appendix A. Supplementary data

Supplementary data to this article can be found online at https://doi.org/10.1016/j.arabjc.2023.105144.

## References

Akhtar, W., Khan, M.F., Verma, G., Shaquiquzzaman, M., Rizvi, M. A., Mehdi, S.H., Akhter, M., Alam, M.M., 2017. Therapeutic evolution of benzimidazole derivatives in the last quinquennial period. Eur. J. Med. Chem. 27 (126), 705–753. https://doi.org/10.1016/j.ejmech.2016.12.010.

Aragón-Muriel, A., Liscano, Y., Upegui, Y., Robledo, S.M., Ramírez-Apan, M.T., Morales-Morales, D., Oñate-Garzón, J., Polo-Cerón, D., 2021. In vitro evaluation of the potential pharmacological activity and molecular targets of new benzimidazole-based schiff base metal complexes. Antibiotics (Basel). 10 (6), 728. https://doi.org/10.3390/antibiotics10060728.

Aroua, L.M., Alhag, S.K., Al-Shuraym, L.A., Messaoudi, S., Mahyoub, J.A., Alfaifi, M.Y., Al-Otaibi, W.M., 2023. Synthesis and characterization of different complexes derived from Schiff base and evaluation as a potential anticancer, antimicrobial, and insecticide agent. Saudi J Biol Sci. 30, (3). https://doi.org/10.1016/j.sjbs.2023.103598 103598.

Ates-Alagoz, Z., 2016. Antimicrobial Activities of 1-H-Benzimidazole-based Molecules. Curr. Top. Med. Chem. 16 (26), 2953–2962. https://doi.org/10.2174/1568026616666160506130226.

Bray, F., Ferlay, J., Soerjomataram, I., Siegel, R.L., Torre, L.A., Jemal, A., 2018. Global cancer statistics 2018: GLOBOCAN estimates of incidence and mortality worldwide for 36 cancers in 185 countries. CA Cancer J. Clin. 68 (6), 394–424. https://doi.org/10.3322/caac.21492.

BrukerSAINT, Bruker AXS Inc. (Madison, Wisconsin, USA, 2012).

Casanova, I., Durán, M.L., Viqueira, J., Sousa-Pedrares, A., Zani, F., Real, J.A., García-Vázquez, J.A., 2018. Metal complexes of a novel heterocyclic benzimidazole ligand formed by rearrangement-cyclization of the corresponding Schiff base. Electrosynthesis, structural characterization and antimicrobial activity. Dalton Trans. 47 (12), 4325–4340. https://doi.org/10.1039/c8dt00532j.

Fontana, R., Marconi, P.C.R., Caputo, A., Gavalyan, V.B., 2022. Novel chitosan-based Schiff Base compounds: chemical characterization and antimicrobial activity. Molecules 27 (9), 2740. https://doi.org/10.3390/molecules27092740.

Galal, SA, Hegab, KH, Kassab, AS, Rodriguez, ML, Kerwin, SM, el-Khamry, AM, el-Diwani, HI, 2009. New transition metal ion complexes with benzimidazole-5-carboxylic acid hydrazides with antitumor activity. Eur J Med Chem 44 (4), 1500–1508. https://doi.org/10.1016/j.ejmech.2008.07.013.

Ghosh, S., 2019. Cisplatin: The first metal based anticancer drug. Bioorg. Chem. 88,. https://doi.org/10.1016/j.bioorg.2019 102925.

Hranjec, M., Starčević, K., Pavelić, S.K., Lučin, P., Pavelić, K., Karminski, Z.G., 2011. Synthesis, spectroscopic characterization and antiproliferative evaluation in vitro of novel Schiff bases related to benzimidazoles. Eur. J. Med. Chem. 46 (6), 2274–2279. https://doi.org/10.1016/j.ejmech.2011.03.008.

Hübschle, C.B., Sheldrick, G.M., Dittrich, B., 2011. ShelXle: a Qt graphical user interface for SHELXL. J. Appl. Cryst. 44 (Pt 6), 1281–1284. https://doi.org/10.1107/S0021889811043202.

Keri, R.S., Hiremathad, A., Budagumpi, S., Nagaraja, B.M., 2015. Comprehensive review in current developments of benzimidazole-based medicinal chemistry. Chem. Biol. Drug Des. 86 (1), 19–65. https://doi.org/10.1111/cbdd.12462.

Keri, R.S., Rajappa, C.K., Patil, S.A., Nagaraja, B.M., 2016. Benzimidazole-core as an antimycobacterial agent. Pharmacol. Rep. 68 (6), 1254–1265. https://doi.org/10.1016/j.pharep.2016.08.002.

Khan, S., Alhumaydhi, F.A., Ibrahim, M.M., Alqahtani, A., Alshamrani, M., Alruwaili, A.S., Hassanian, A.A., Khan, S., 2022. Recent advances and therapeutic journey of schiff base complexes with selected metals (Pt, Pd, Ag, Au) as potent anticancer agents: a review. Anticancer Agents Med Chem. 22 (18), 3086–3096. https://doi.org/10.2174/1871520622666220511125600.

Köberle, B., Tomicic, M.T., Usanova, S., Kaina, B., 2010. Cisplatin resistance: preclinical findings and clinical implications. BBA 1806 (2), 172–182. https://doi.org/10.1016/j.bbcan.2010.07.004.

Kostova, I., Saso, L., 2013. Advances in research of Schiff-base metal complexes as potent antioxidants. Curr. Med. Chem. 20 (36), 4609–4632. https://doi.org/10.2174/09298673113209990149.

Krause, L., Herbst-Irmer, R., Sheldrick, G.M., Stalke, D., 2015. Comparison of silver and molybdenum microfocus X-ray sources for single-crystal structure determination. J. Appl. Crystallogr. 48 (Pt 1), 3–10. https://doi.org/10.1107/S1600576714022985.

Kumar, P., Nagarajan, A., Uchil, P.D., 2018. Analysis of Cell Viability by the MTT Assay. Cold Spring Harb Protoc. 2018 (6). https://doi.org/10.1101/pdb.prot095505.

Kumaravel, G., Ponya Utthra, P., Raman, N., 2018. Exploiting the biological efficacy of benzimidazole based Schiff base complexes with l-Histidine as a co-ligand: combined molecular docking, DNA interaction, antimicrobial and cytotoxic studies. Bioorg. Chem. 77, 269–279. https://doi.org/10.1016/j.bioorg.2018.01.024.

Magd-El-Din, A.A., Mousa, H.A., Labib, A.A., Hassan, A.S., Abd El-All, A.S., Ali, M.M., El-Rashedy, A.A., El-Desoky, A.H., 2018. Benzimidazole - Schiff bases and their complexes: synthesis, anticancer activity and molecular modeling as Aurora kinase inhibitor. Z. Naturforsch., C: J. Biosci. 73 (11–12), 465–478. https://doi.org/10.1515/znc-2018-0010.

Paul, A., Anbu, S., Sharma, G., Kuznetsov, M.L., Koch, B., Guedes da Silva, M.F., Pombeiro, A.J., 2015. Synthesis, DNA binding, cellular DNA lesion and cytotoxicity of a series of new benzimidazole-based Schiff base copper(II) complexes. Dalton Trans. 44 (46), 19983–19996. https://doi.org/10.1039/c5dt02880a.

Peng, W., Zhang, S., Zhou, W., Zhao, X., Wang, K., Yue, C., Wei, X., Pang, S., Dong, W., Chen, S., Chen, C., Yang, Q., Wang, W., 2022. Layered double hydroxides-loaded sorafenib inhibit hepatic stellate cells proliferation and activation in vitro and reduce fibrosis in vivo. Front. Bioeng. Biotechnol. 27, (10). https://doi.org/10.3389/fbioe.2022.873971 873971.

Reshma, R., Selwin Joseyphus, R., Arish, D., Reshmi Jaya, R.J., Johnson, J., 2022. Tridentate imidazole-based Schiff base metal complexes: molecular docking, structural and biological studies. J. Biomol. Struct. Dyn. 40 (18), 8602–8614. https://doi.org/10.1080/07391102.2021.1914171.

Sirim, M.M., Krishna, V.S., Sriram, D., Unsal, T.O., 2020. Novel benzimidazole-acrylonitrile hybrids and their derivatives: Design, synthesis and antimycobacterial activity. Eur. J. Med. Chem. 15, (188). https://doi.org/10.1016/j.ejmech.2019.112010 112010.

Skrodzki, M., Patroniak, V., Pawluć, P., 2021. Schiff Base Cobalt(II) complex-catalyzed highly markovnikov-selective hydrosilylation of alkynes. Org. Lett. 23 (3), 663–667. https://doi.org/10.1021/acs.orglett.0c03721.

Sun, C.Y., Zhang, Q.Y., Zheng, G.J., Feng, B., 2019. Phytochemicals: current strategy to sensitize cancer cells to cisplatin. Biomed. Pharmacother. 110, 518–527. https://doi.org/10.1016/j.biopha.2018.12.010.

Tahlan, S., Narasimhan, B., Lim, S.M., Ramasamy, K., Mani, V., Shah, S.A.A., 2019. 2-Mercaptobenzimidazole Schiff Bases: Design, Synthesis, Antimicrobial Studies and Anticancer Activity on HCT-116 Cell Line. Mini Rev. Med. Chem. 19 (13), 1080–1092. https://doi.org/10.2174/1389557518666181009151008.

Torre, L.A., Siegel, R.L., Ward, E.M., Jemal, A., 2016. Global cancer incidence and mortality rates and trends–an update. Cancer Epidemiol. Biomark. Prev. 25 (1), 16–27. https://doi.org/10.1158/1055-9965.

Wang, R., Liu, T., Chen, J., Zhang, D., 2022. Paradol induces cell cycle arrest and apoptosis in glioblastoma cells. Nutr. Cancer 74 (8), 3007–3014. https://doi.org/10.1080/01635581.2022.2028866.

Xu, Y., Shi, Y., Lei, F., Dai, L., 2020. A novel and green cellulose-based Schiff base-Cu (II) complex and its excellent antibacterial activity. Carbohydr. Polym. 15, (230). https://doi.org/10.1016/j.carbpol.2019.115671 115671.

Yadav, G., Ganguly, S., 2015. Structure activity relationship (SAR) study of benzimidazole scaffold for different biological activities: a mini-review. Eur. J. Med. Chem. 5 (97), 419–443. https://doi.org/10.1016/j.ejmech.2014.11.053.